Effect of Elastic Collisions on Energy Deposition by Electrons in Water

Jay A. LaVerne* and Simon M. Pimblott

Radiation Laboratory, University of Notre Dame, Notre Dame, Indiana 46556

Received: January 16, 1997; In Final Form: April 14, 1997[⊗]

Monte Carlo simulation methods have been used to evaluate the effects of elastic collisions on the transport of 0.1, 1, 10, and 100 keV energy electrons in water. The simulations show that transport-related phenomena in the direction axial (parallel) to the initial direction of travel are more dependent on elastic processes than those in the radial (perpendicular) direction. A decrease in the total elastic cross section to 10% of its gas phase value increases the mean axial penetration depths and the maximum of the axial energy deposition gradients by as much as a factor of 2. The most pronounced effects are observed for electrons of 100 eV energy where even the mean radial penetrations are doubled. Except for these low energies, the mean radial penetrations and the radial energy deposition gradients are relatively unaffected by elastic processes, implying that these parameters are mainly determined by inelastic collisions.

Introduction

Knowledge of the spatial distribution of the energy deposited by energetic electrons in their passage through matter is fundamental to the assessment of radiation damage. Several sophisticated Monte Carlo simulation techniques for modeling the trajectories of electrons in water and in aqueous solutions have been developed.[1−5] These codes use extensive arrays of cross sections for which no experimental values are known in the condensed phase. Obviously, the success of these codes for predicting the paths of electrons and their energy loss characteristics is strongly dependent on the choice of the cross-sectional data. Most of the discussions on cross sections have focused on the inelastic processes, especially on the validity of using liquid density gaseous cross sections to model liquid water. While inelastic processes are very important in determining energy losses and rightly deserve scrutiny, there has been no analysis of the effects of elastic processes on the transport of electrons in water. This work examines the effects of elastic collisions on electron transport in water using Monte Carlo simulations for electrons of 0.1−100 keV energy.

A complete analysis of the transport of energetic electrons and all of the daughters produced by ionizing collisions until the electrons are sufficiently slowed to the point that further electronic collisions are not possible involves a wide range of energies. There have been a number of experimental studies in gaseous water on the elastic scattering cross sections of electrons from a few electronvolts to about 1 keV. [6−10] Some of the experiments provide limited information on differential cross sections; however, the Monte Carlo codes require values over all angles at each energy. Therefore, a common procedure in modeling is to make use of semiempirical models to estimate elastic cross sections. Mozumder used a Thomas−Fermi model which is valid for atoms.[11] Spencer modified the Rutherford cross section to include screening of the nuclear field by the electrons.[12] The magnitude of the nuclear screening was first estimated by Molière[13] and more extensively studied by Bethe.[14] In practice, it has been found that the screening parameter is best varied to fit the experimental values of the total elastic cross section.[15,16] All of the Monte Carlo codes use this procedure in one form or other. While this approach ensures reasonable values for the total elastic cross section, it does not necessarily predict correct differential cross sections. It also does not address the possible effect of phase on elastic collisions. This work examines the influence of different angular dependences of elastic cross sections on electron transport as well as effects due to variation in the total elastic cross section.

In this study, Monte Carlo simulation techniques are used for predicting the spatial distribution of the energy loss events along tracks of energetic electrons in water.[5] The simulation methodology and cross sections are discussed in the next section. A discussion of the results calculated for a variety of elastic cross sections then follows. The final section summarizes the comments made and conclusions drawn.

Methodology

Track Structure Simulation. A complete description of the methodology for simulating the trajectory of an electron as it loses energy in water has been presented elsewhere.[5] Briefly, the path of an electron of defined initial energy and direction is modeled using a collision by collision approach. The distance between two consecutive collisions is determined by using a uniformly distributed random number to sample from a probability distribution constructed using Poisson statistics and the mean free path. The new electron position is determined from the distance traveled and the original directional coordinates. A second random number is then used to determine whether the collision involves an energy transfer by comparing the ratio of the inelastic cross section with the sum of the inelastic and elastic cross sections. Inelastic events are treated in a similar manner to determine whether the collision led to ionization, excitation, or vibration of the medium molecule. The magnitude of energy loss in the collision is evaluated, and the energy of the incident electron is modified accordingly. Changes in the trajectory of the incident electron are calculated from the kinematics in inelastic collisions and from the appropriate angular distribution in elastic collisions. Successive generations of secondary electrons created with energy greater than 25 eV are degraded in the same manner until their energy falls below 25 eV, at which point progression of the trajectory of the primary electron is continued. The simulations proceed until the energy of the primary electron drops below 25 eV. The lower limit of 25 eV was chosen because the inelastic cross section decreases rapidly with energies below this value and other transport phenomenon, such as isotropic thermalization, become more dominant.[5]

[⊗] Abstract published in *Advance ACS Abstracts,* June 1, 1997.

S1089-5639(97)00227-2 CCC: $14.00 © 1997 American Chemical Society

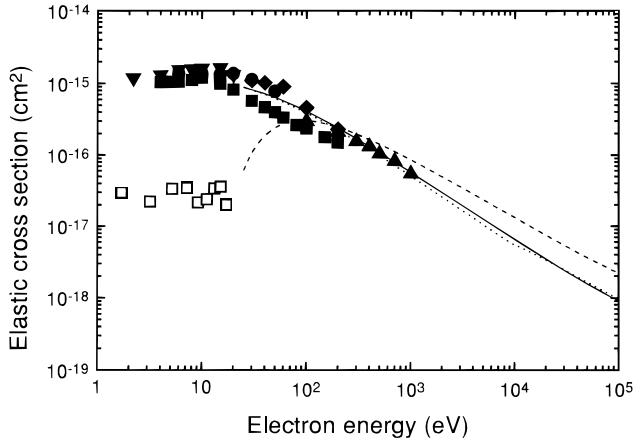

Figure 1. Effect of electron energy on the total cross section for elastic collisions of electrons in water: screened Rutherford cross section using eq 4a (dotted line), screened Rutherford cross section using eq 4b (solid line); experiment, (■) ref 6, (●) ref 7, (▲) ref 8, (▼) ref 9, and (◆) ref 10. Total electronic cross sections are shown as a dashed line, ref 5, and experimental elastic cross section in ice (□), ref 18.

Typically, 10^4-10^5 total simulations are performed for a given primary electron energy. All electronic, ionization, and vibration−rotation cross sections are the same as used previously for the liquid phase of water.[5]

Elastic Cross Sections. Experimental values for the total elastic cross-section for gaseous water are shown in Figure 1 as a function of electron energy.[6−10] Also shown in the figure are the theoretical cross sections obtained by evaluating

$$\sigma_{\text{elastic}} = 2\pi\int_0^{\pi}\sigma'(\theta, E)\sin\theta\,\mathrm{d}\theta \qquad (1)$$

using two different formulations for the Molière screening of the Rutherford differential cross section, $\sigma'(\theta,E)$. The angular dependence of the differential elastic cross sections has the form

$$\sigma'(\theta,E) = (Z^2 + Z)e^4/(p^2v^2(1 - \cos\theta + 2\eta)^2) \qquad (2)$$

where p, e, and v are the electron momentum, charge, and velocity, respectively. In this expression, Z is the total number of electrons per molecule and η is the nuclear screening parameter given by the following expression:

$$\eta = Z^{2/3}\eta_c/(T(T+2)) \qquad (3)$$

Here, T is the kinetic energy of the electron in units of mc^2 and η_c is a fitted parameter.

Using a formalism originally suggested by Berger, LaVerne and Mozumder fitted eq 1 to the available experimental data and found that for water

$$\eta_c = 1.13 + 3.76(Z/(137\beta))^2 \qquad (4a)$$

subject to the condition that $\eta_c < 1.7$.[17] Without the added constraint, the Molière screening parameter causes the total cross section to deviate significantly from the data and quickly decrease to zero at energies less than about 10 keV. Unfortunately, it can be seen in Figure 1 that this restriction introduces a cusp in the calculated cross section at about 10 keV. A different formalism suggested by Grosswendt and Waibel was also scaled to the experimental data using

$$\eta_c = 1.64 - 0.0825\ln(Tmc^2) \qquad (4b)$$

which results in a smooth curve for the energy dependence of the total cross section. Both formalisms for the screening parameter fit the data well and predicte the same angular dependence. The one due to Grosswendt and Waibel is used in this work because it offers a smooth energy dependence for the total elastic cross section.

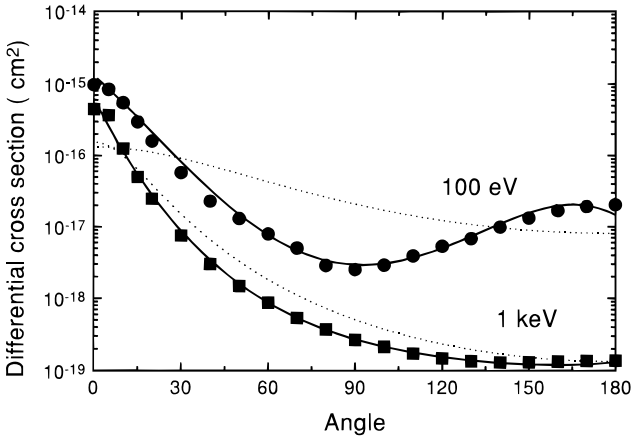

Figure 2. Angular dependence of the cross section for elastic collisions of 100 eV and 1 keV energy electrons in water: screened Rutherford cross section, equation 4b (dotted lines); polynomial interpolation of experiments, eq 5 (solid lines); experimental, ref 8, (●) 100 eV, (■) 1 keV.

A comparison of the experimental data and the calculated differential cross sections is shown Figure 2 for a 100 eV and a 1 keV energy electron. Even though the total elastic cross sections are similar, the angular dependence of the experimental data for low-energy electrons does not correspond to that predicted by eq 2. The modified Rutherford cross section predicts too little forward scattering and a more isotropic angular distribution than observed experimentally. In order to fully exploit the available experimental data, an alternative description of the angular dependence was developed.[5] The available experimental data were critically evaluated and fitted using the polynomial function

$$\sigma'(\theta,E) = a_0 + a_1\theta + a_2\theta^2 + a_3\theta^3 + a_4\theta^4 \qquad (5)$$

where the coefficients a_0, a_1, a_2, a_3, and a_4 depend on electron energy. The energy dependence of each of these parameters was again fit with a fourth-order polynomial. Such a procedure provides a method that allows for the fast and accurate computation of the differential cross section as a function of θ and E. The differential elastic cross sections interpolated using this treatment are included in Figure 2. The interpolated cross sections reproduce the experimental measurements significantly better than those calculated using the Molière screening parameter.

Most of the following discussion will consider the effects due to elastic processes; however, the magnitude of the elastic cross section with respect to the total inelastic cross section is important. For comparison, Figure 1 contains the energy dependence of the electronic contribution to the inelastic cross section as obtained from the dipole oscillator strength distribution of liquid water.[5]

The Monte Carlo calculations were performed with four different assumptions for the elastic cross section: (a) *experimental*, the total elastic cross section as obtained from the best fits to the experimental data, i.e. using eqs 1, 2, 3, and 4b with the angular dependences determined by eq 5; (b) *Rutherford*, the same total elastic cross section as in (a) but with angular dependences as determined from the Molière screening parameter, i.e. using eqs 2, 3, and 4b; (c) *reduced experimental*, the

total elastic cross sections set to 10% of the experimental values with the same angular dependences as in (a); and (d) *no elastic*, the total elastic cross sections set to zero. All inelastic cross sections and other parameters were the same in all of the calculations.

Results and Discussion

Monte Carlo track structure simulations are well-suited for exploring the effects of elastic collisions because of the detailed spatial information they provide. Simple deterministic modeling techniques which give only energy loss parameters are not suitable for this task. For instance, the path length and stopping power are not affected by the elastic collisions since these events do not result in energy loss. Simulations in which the elastic collisions are ignored, i.e. $\sigma_{elastic}$ is set to zero, do not affect the predictions for these parameters. The most noticeable effects of elastic collisions are on those properties that depend on the trajectories of the electron. These parameters include the range, the dose, and the energy loss gradients of the electron. Each of the following sections will look into these areas separately.

Since the purpose of the present work is to examine the effects of elastic collisions on electron transport, the elastic cross sections were varied systematically and the changes in the results recorded. The elastic cross sections obtained by the best fit to the gas phase experimental results for both the total cross section and its angular dependence are assumed to be representative of reality and used as the standard for comparison. This type of cross section will be denoted as "experimental" for the liquid even though it is known to be strictly correct only for the gas phase. The effects of the angular distribution on electron transport properties are examined by performing identical sets of calculations with the same total elastic cross section only using the angular distribution predicted by the Rutherford cross section with the Molière screening parameter, eqs 2, 3, and 4b.

The effect of condensation on elastic cross sections is not known as no information on elastic cross sections in liquid water is presently available. It is expected that the effect of condensation will be small since these collisions are dominated by the interaction of the incident electron with the nuclei of the medium. However, Michaud and Sanche[18] have measured total elastic cross sections in ice and found them to be more than an order of magnitude lower than in the gas phase; cf. Figure 1. The cross sections in ice represent lower limits because the experimental technique does not take into account elastic processes with small angular deflections. Other models for liquid water have assumed a more conservative 60% decrease in the total cross section from the gas to liquid phase.[2,3] In this work, it was assumed that the maximum effect of condensation on the total elastic cross section is to reduce its magnitude to 10% of the value for the gas phase. The angular dependence was assumed to remain the same as in the gas phase. Finally, an estimate of the total effect due to elastic processes was obtained by setting the elastic cross section to zero.

Range Distributions. Track structure simulations were used to predict four different distances traveled by an electron: (i) the path length, (ii) the vector distance $|\mathbf{X}_f - \mathbf{X}_i|$ between the initial position ($\mathbf{X}_i$) and final position ($\mathbf{X}_f$), (iii) the absolute value of the radial component of the vector $\mathbf{X}_f - \mathbf{X}_i$ (perpendicular to the initial electron trajectory), and (iv) the axial component of the vector $\mathbf{X}_f - \mathbf{X}_i$ (parallel to the initial electron trajectory). By definition, elastic processes make no contribution to the total path length. Elastic collisions change the direction of motion, but the distance traversed between inelastic collisions remains the same. Of course, the calculations showed no effect on path length when the elastic cross section was set to zero.

TABLE 1: Mean Radial, Axial, and Vector Penetrations for 0.1, 1, 10, and 100 keV Electron in Water Using Different Elastic Cross Sections (in Units of nm)

	100 eV	1 keV	10 keV	100 keV
		Radial		
Rutherford	2.23	21.0	9.86×10^2	5.48×10^4
exptl	2.79	22.4	9.81×10^2	5.50×10^4
$\sigma_{el} = 0.1$ (exptl)	5.18	23.4	1.03×10^3	5.62×10^4
$\sigma_{el} = 0$	6.65	23.8	9.50×10^2	5.28×10^4
		Axial		
Rutherford	1.68	21.5	1.02×10^3	5.60×10^4
exptl	2.25	25.9	9.61×10^2	5.60×10^4
$\sigma_{el} = 0.1$ (exptl)	4.47	40.9	1.82×10^3	1.02×10^5
$\sigma_{el} = 0$	5.74	44.8	2.06×10^3	1.12×10^5
		Vector		
Rutherford	3.02	32.5	1.53×10^3	8.44×10^4
exptl	3.88	36.8	1.48×10^3	8.45×10^4
$\sigma_{el} = 0.1$ (exptl)	7.43	49.4	2.18×10^3	1.21×10^5
$\sigma_{el} = 0$	9.55	52.7	2.33×10^3	1.28×10^5

The mean radial penetration is given in Table 1 for 0.1, 1, 10, and 100 keV electrons in liquid water. For electrons of 1 keV energy and above, elastic processes have very little effect on the radial penetration. Radial penetration is determined mainly by hard inelastic (ionization) events which alter the particle trajectory due to the kinematics of the collision. At 100 eV energy, elastic collisions reduce the mean radical penetration by more than a factor of 2. It can be seen in Figure 1 that at this energy the elastic and inelastic cross sections are of similar magnitude. Below 100 eV the inelastic cross section decreases very rapidly, and at low electron energies the predominant type of collision is elastic. Therefore, a strong dependence of the radial penetration on the magnitude of the total elastic cross section is expected. Only a minimal dependence of the radial penetration on the angular distribution is apparent at electron energies greater than 1 keV.

No phase effect on the radial penetration is expected for electrons above about 1 keV energy. However, since the magnitude of the elastic cross section is very important in determining the radial penetration of lower energy electrons, an observable phase effect is possible. This effect may lead to an increase in the radial penetration by as much as a factor of 2 from the gas to the condensed phases. Of course, the observable effect of elastic cross section depends on the relative magnitude of the elastic to the inelastic cross section.

The mean axial penetration is strongly dependent on elastic collisions at all electron energies. Table 1 shows the calculated mean axial penetrations for the four electron energies using each of the elastic cross sections. Decreasing the experimental elastic cross sections to 10% doubles the mean axial penetration. A further increase in penetration is observed for the lower energies if the elastic cross section is completely removed. It appears that elastic processes can decrease the penetration by at least a factor of 2 at all of the energies examined here. Consequently, condensation is expected to have a rather strong effect on the axial penetration if the elastic cross section in the liquid phase differs significantly from its gas phase value.

At energies above 10 keV the angular distribution of the elastic cross section has virtually no effect on the axial penetration. This result is not too surprising since the angular dependence of the screened Rutherford cross section is very similar to experimental observations. Even at 1 keV the angular dependences are very similar; cf. Figure 2. However, at progressively lower energies, the more forward peaked experimental cross sections lead to progressively longer axial penetrations when compared to the results obtained using screened Rutherford cross sections. A 100 eV electron exhibits more

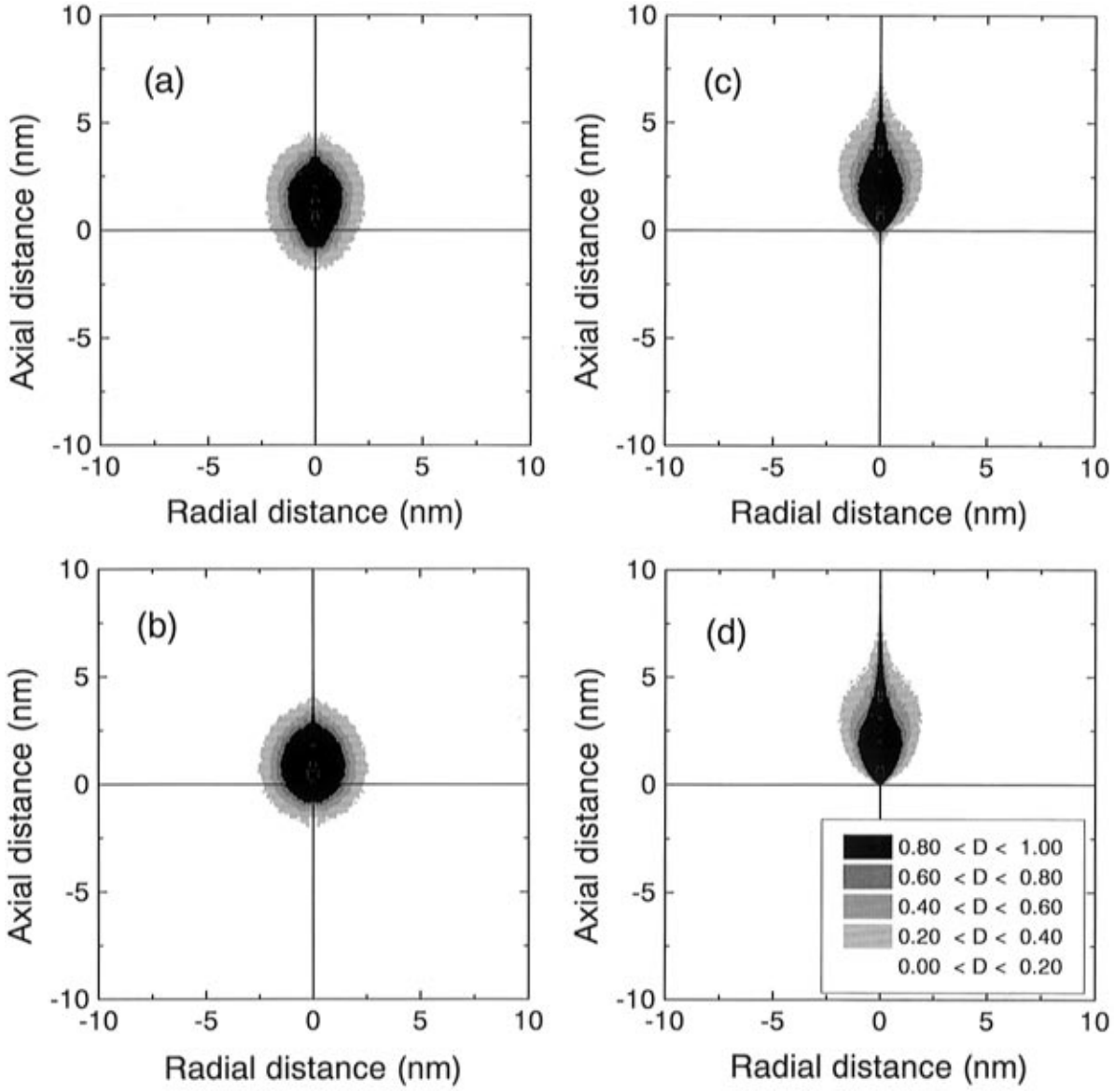

Figure 3. Energy deposition density, *D* (eV/nm), contours for 100 eV energy electrons for the various formalisms of elastic cross sections: (a) experimental gas phase values; (b) same total cross section as in (a) with angular dependence predicted by a screened Rutherford cross section; (c) total cross sections of (a) reduced to 10% with same angular dependence; (d) elastic cross section set to zero.

than a 30% change in axial penetration for the two angular dependences examined compared to a 17% change for a 1 keV electron and a 4% change for a 10 keV electron.

The mean vector penetration is a composite of both the radial and axial penetrations. Therefore, its dependence on elastic processes will be strongly affected by which of these components is the dominant one. As seen in Table 1, the magnitudes of the mean axial and radial penetrations depths are about the same at all energies. It is observed that the mean vector penetration is dependent on elastic processes, but not quite as much as the mean axial penetration. At high electron energies, the mean vector penetration increases by about 50% on decreasing the elastic cross section by an order of magnitude. The complete elimination of the elastic cross section does not have much more of an effect. Electrons of 100 eV and lower are more profoundly effected by elastic processes. Decreasing the elastic cross section to 10% of the experimental value increases the mean vector range by a factor of 2. Setting the elastic cross section to zero increases the mean vector penetration by more than a factor of 3. Low-energy electrons are mainly responsible for the formation of the nonhomogeneous distributions of reactive species, spurs, produced by high-energy ionizing radiation and therefore are fundamental in determining observable radiation chemical kinetics. If the thermalization distance of low-energy electrons is small compared to the mean vector penetration, then the physical size of spurs estimated using gas phase cross sections may be somewhat smaller than reality.[19] Of course, thermalization distances cannot be ignored, but they are not addressed in this work.

The mean vector penetration shows very little angular dependence at high electron energies. Even at 100 eV energy, the increase in penetration is only 30% for the more forward peaked experimental elastic cross sections. For the most part, the dependence of the mean vector penetration on the angular distribution is the same as found with the mean axial penetration.

Energy Deposition Density. The ranges of electrons are important for many applications, but in radiolysis the overall shapes of the energy deposition distributions are perhaps more significant in determining the chemistry. Previous calculations[5] have shown that at low electron energies the energy deposition distribution is nearly spherical centered about the origin. With increasing electron energy the distribution progresses through an ellipsoidal to more of a dumbbell shape. This change in

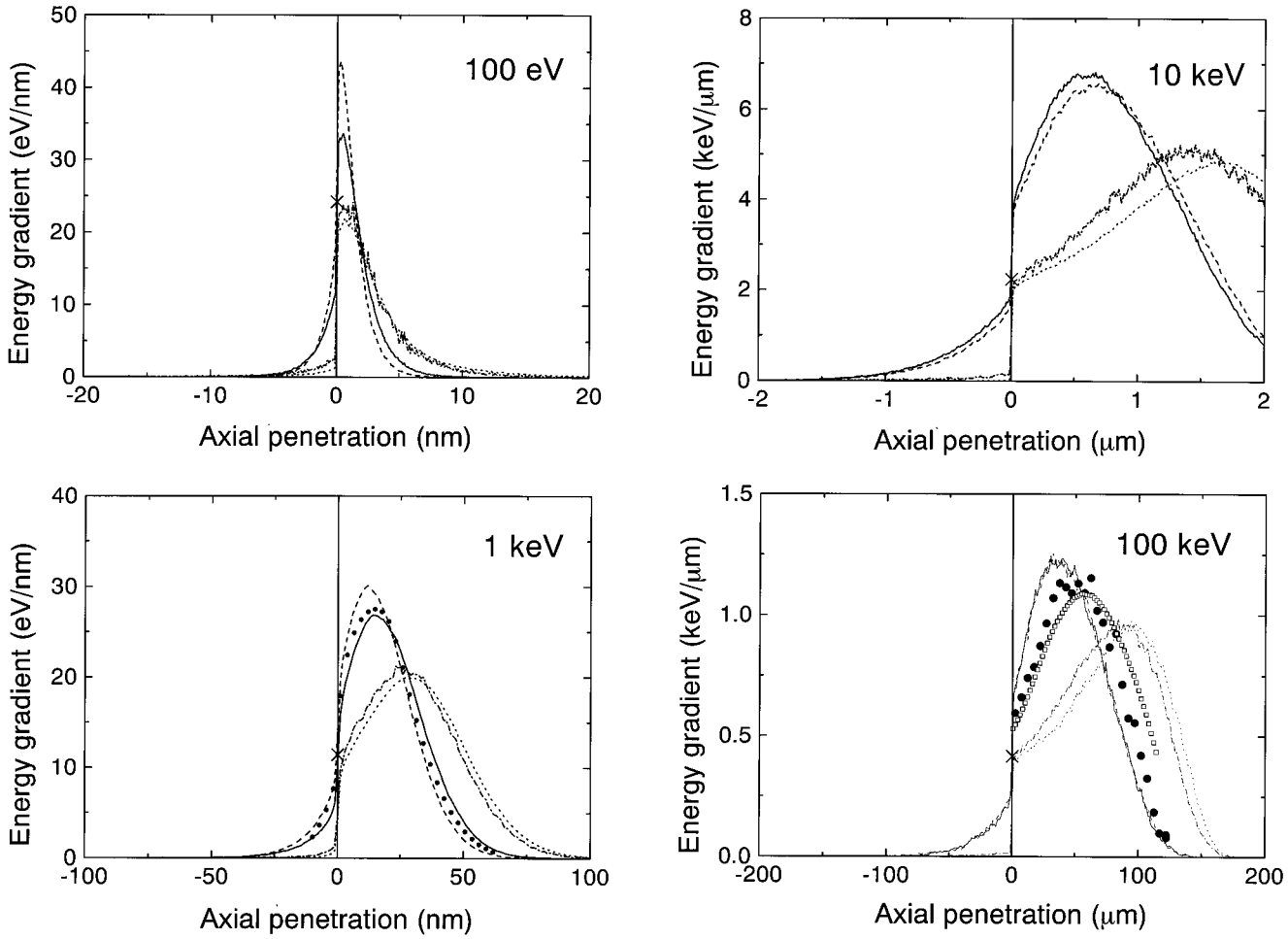

Figure 4. Energy deposition gradient as a function of axial penetration for 0.1, 1, 10, and 100 keV electrons using the various formalisms of elastic cross sections: (a) (solid line) experimental gas phase values; (b) (dashed line) same total cross section as in (a) with angular dependence predicted by a screened Rutherford cross section; (c) (dot-dash line) total cross sections of (a) reduced to 10% with same angular dependence; (d) (dotted line) elastic cross section set to zero. The initial stopping powers at each energy are given by (×), and the gradients from other work are at 1 keV (●) ref 20 and at 100 keV (●) ref 21 and (□) ref 22.

shape is due to the increase in the inelastic cross section with respect to the elastic cross section at higher energies. At very high electron energies, the inelastic cross section is much greater than the elastic one, and most of the energy density is located in the forward direction. With low-energy electrons the relative magnitudes of the cross sections are reversed, and the track is much more spherical due to the high number of large-angle scattering processes (both elastic and inelastic).

The predicted effects of the various elastic cross sections on the penetration of an electron are most pronounced at lower energies. Low-energy electrons are centrally important in radiolysis processes so an examination of the effects of elastic processes on energy deposition density will focus on these energies. Figure 3 shows a contour plot of the variation in energy deposition using the four formalisms for the elastic cross section. Experimental gas phase cross sections predict a spherical distribution that is slightly elongated in the forward axial direction. The relatively forward peaked angular dependence at low energies may account for this small bias in direction. It is observed that the use of the more isotropic screened Rutherford cross section results in a more spherical distribution. The centers of both distributions are also slightly displaced in the forward axial direction. Apparently, the memory of the initial forward direction of the electron is maintained even at these low energies.

Reducing the elastic cross section by a factor of 10 or setting it to zero appears to have about the same effect on the energy deposition distributions. Instead of a spherical geometry the distributions are more teardrop shaped. The radial penetration results suggest that the width of the distribution could increase by as much as a factor of 2 on the elimination of the elastic cross section. However, the energy distributions appear to be slightly narrower or at least unaffected in the radial direction on reducing the value of the total elastic cross section. This apparent discrepancy is due to the fact that the penetration only describes the final position of the attenuated electron, while the energy distribution shows the spatial location of energy attenuation. A reduction of the elastic cross section values seems to stretch the energy distributions more along the axial axis. The main region of energy deposition is close to the origin for all the elastic cross sections because the rate of energy loss of the electron decreases as it slows.

Energy Loss Gradient. A quantitative measure of the energy deposition gradient of an electron in the plane of its initial motion can be obtained by integration of the radial dose distribution in the radial direction. A similar summation in the axial direction gives the radial dependence. The results of such calculations are shown in Figures 4 and 5 where the gradient of energy deposition in the axial and radial directions are plotted as a function of the respective penetration for 0.1, 1, 10, and 100 keV electrons. Each figure shows the results due to the various formalisms for the elastic cross sections. Figure 4 also shows the initial stopping powers for the four electron energies and the energy deposition gradients of Turner et al.[20] for

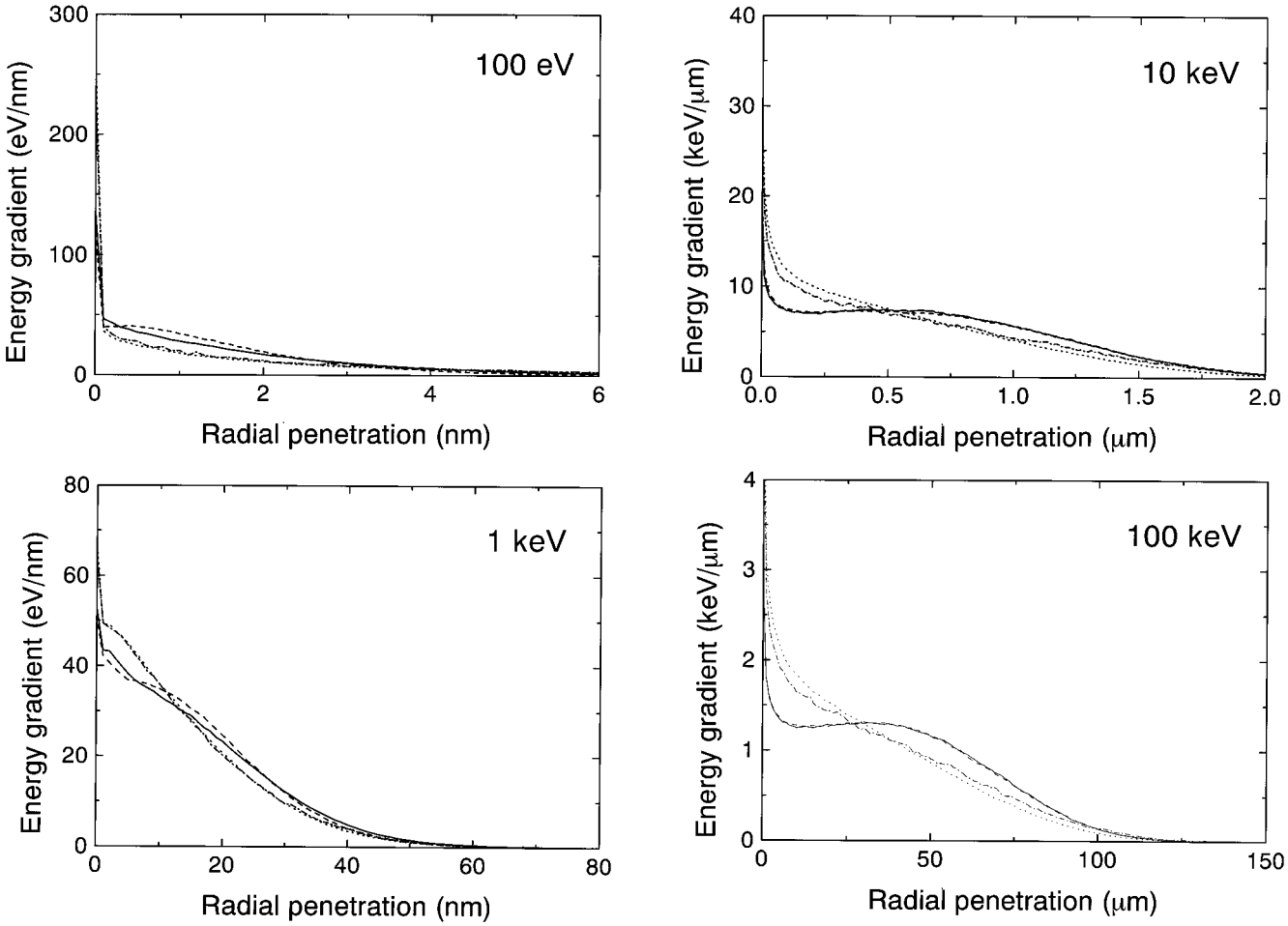

Figure 5. Energy deposition gradient as a function of radial penetration for 0.1, 1, 10, and 100 keV electrons using the various formalisms of elastic cross sections; line types are the same as in Figure 4.

electrons of 1 keV energy and for electrons of 100 keV energy by Hamm et al.[21] and Kobetich and Katz.[22]

The position of the maximum of the distributions for the energy loss gradient in the axial direction are very similar for the experimental gas phase elastic cross sections, and the screened Rutherford cross sections at all electron energies. At low energies the width of the distribution is smaller for the Rutherford cross sections, and it gradually increases relative to that predicted using experimental cross sections as the electron energy increases. There is virtually no difference between the two distributions at the highest energies.

Very little difference in the energy gradient distributions in the axial direction is observed by setting the cross section to zero or to 10% of the experimental value, although both of these distributions are very different from that predicted using experimental elastic cross sections. At low electron energies both of the distributions are peaked at about the same position as with the experimental cross sections. With increasing electron energy the distributions for the reduced values of the total elastic cross section shift to greater axial penetration depths than observed with experimental cross sections. At the highest energies the peak positions of the distributions can vary by more than a factor of 2. This magnitude corresponds roughly to the variation in the mean axial penetration observed in Table 1. The large increase in the mean axial penetration upon reduction of the elastic cross section for 100 eV energy electrons is not as pronounced in the distributions for the energy loss gradients. The energy loss gradient with no elastic cross section is slightly skewed to large penetration values.

Backscattering of electrons due to elastic processes can occur by a succession of small-angle scattering events or a few large angle ones. At energies above 1 keV most of the backscattering is due to elastic processes. Removal of the elastic processes results in almost no backscattering. Generally, the forward momentum of the electron in the initial part of its path carries it sufficiently far from the origin that later collisions after the electron energy has decreased substantially do not return it to the origin. At low electron energies back scattering is due to both elastic and inelastic processes.

The energy gradients in the radial direction seem to be somewhat independent of the elastic cross section chosen for all energy electrons; cf. Figure 5. This result is probably predictable from the variations of the mean radial penetrations listed in Table 1. Reduction of the magnitude of the cross section produces an energy gradient with a monotonic decrease with increasing radial penetration. The experimental cross sections show a peak value for the energy gradient at the origin, but another maximum is displaced from the origin. The cause of this second maximum is easily explained by considering the radial dose distribution. As the distance along the direction of the original trajectory increases, the radial position of greatest density moves away from the origin. The possible effects of phase on the energy gradient in the radial direction are expected to be negligible.

Summary

Monte Carlo simulation methods have been used to evaluate the effects of elastic cross sections on the transport of 0.1, 1,

10, and 100 keV energy electrons in liquid water. Condensation is expected to decrease the value of the total elastic cross section if it has any effect at all. The simulations predict that a decrease in the total elastic cross section to 10% of its gas phase value increases the mean axial penetration depth and the maximum of the axial energy deposition gradients by as much as a factor of 2. The most pronounced effects are observed for 100 eV energy electrons where even the mean radial penetration is doubled. Except for these low energies, the mean radial penetration and the radial energy deposition gradient are relatively unaffected by elastic processes. Of course, the magnitude of the condensation effects will depend on the relative values of the total cross sections for the gas and liquid phases. The effects of phase on the total elastic cross section considered in this work are suggested by experiments in ice[18] and represent the maximum changes possible. Furthermore, these calculations are restricted to the transport of electrons above 25 eV. Thermalization phenomena may significantly influence the transport of low-energy electrons. Consequently, the effects of elastic collisions discussed here may be substantially moderated when describing short time radiation chemistry.

Acknowledgment. The research described was supported by the Office of Basic Energy Sciences of the U.S. Department of Energy. This is Contribution NDRL-3977 from the Notre Dame Radiation Laboratory.

References and Notes

(1) Zaider, M.; Brenner, D. J.; Wilson, W. E. *Radiat. Res*. **1983**, *95*, 231.

(2) Paretzke, H. G.; Turner, J. E.; Hamm, R. N.; Wright, H. A.; Ritchie, R. H. *J. Chem. Phys*. **1986**, *84*, 3182.

(3) Paretzke, H. G.; Turner, J. E.; Hamm, R. N.; Ritchie, R. H.; Wright, H. A. *Radiat. Res*. **1991**, *127*, 121.

(4) Hill, M. A.; Smith, F. A. *Radiat. Phys. Chem*. **1994**, *43*, 265.

(5) Pimblott, S. M.; LaVerne, J. A.; Mozumder, A. *J. Phys. Chem*. **1996**, *100*, 8595.

(6) Danjo, A.; Nishimura, H. *J. Phys. Soc. Jpn*. **1985**, *54*, 1224.

(7) Johnstone, W. M.; Newell, W. R. *J. Phys. B* **1991**, *24*, 3633.

(8) Katase, A.; Ishibashi, K.; Matsumoto, Y.; Sakae, T.; Maezono, S.; Murakami, E.; Watanabe, K.; Maki, H. *J. Phys. B* **1986**, *19*, 2715.

(9) Shyn, T. W.; Cho, S. Y. *Phys. Rev. A* **1987**, *36*, 5138

(10) Shyn, T. W.; Grafe, A. *Phys. Rev. A* **1992**, *46*, 4406.

(11) Mozumder, A. In *Proceedings of the Third Tihany Symposium on Radiation Chemistry*; Dobo, J., Hedvig, P., Eds.; Akademiai Kiado: Budapest; 1972, p 1123.

(12) Spencer, L. V. *Phys. Rev*. **1955**, *98*, 1597.

(13) Molière, G. Z. *Naturforsch.* **1947**, *2A*, 133; **1948**, *3A*, 78.

(14) Bethe, H. A. *Phys. Rev*. **1953**, *89*, 1256.

(15) Berger, M. J. In *Proceedings of the Fourth Symposium on Microdosimetry*; Booz, J., Ebert, H. G., Eikel, R., Waker, A., Eds.; Commision of the European Communities: Luxembourg, 1974; p 695.

(16) Grosswendt, B.; Waibel, E. *Nucl Instrum. Methods* **1978**, *155*, 145.

(17) LaVerne, J. A.; Mozumder, A. *Radiat. Res.* **1983**, *96*, 219.

(18) Michaud, M.; Sanche, L. *Phys. Rev. A* **1987**, *36*, 4672.

(19) LaVerne, J. A.; Mozumder, A. *Radiat. Phys. Chem*. **1984**, *23*, 637.

(20) Turner, J. E.; Paretzke, H. G.; Hamm, R. N.; Wright, H. A.; Ritchie, R. H. *Radiat. Res*. **1982**, *92*, 47.

(21) Hamm, R. N.; Wright, H. A.; Katz, R.; Turner, J. E.; Ritchie, R. H. *Phys. Med. Biol*. **1978**, *23*, 1149.

(22) Kobetich, E. J.; Katz, R. *Nucl. Instrum. Methods* **1969**, *71*, *226*.